Mitochondrial membrane potential decrease caused by loss of PINK1 is not due to proton leak, but to respiratory chain defects

Taku Amo [a,1], Shigeto Sato [b], Shinji Saiki [b], Alexander M. Wolf [a], Masaaki Toyomizu [c], Clement A. Gautier [d], Jie Shen [d], Shigeo Ohta [a], Nobutaka Hattori [b,*]

[a] Department of Biochemistry and Cell Biology, Institute of Development and Aging Sciences, Graduate School of Medicine, Nippon Medical School, 1-396 Kosugi-cho, Nakahara-ku, Kawasaki 211-8533, Japan
[b] Department of Neurology, Juntendo University School of Medicine, 2-1-1 Hongo, Bunkyo-ku, Tokyo 113-8421, Japan
[c] Animal Nutrition, Life Sciences, Graduate School of Agricultural Science, Tohoku University, 1-1 Tsutsumidori-Amamiyamachi, Aoba-ku, Sendai 981-8555, Japan
[d] Center for Neurologic Diseases, Brigham and Women's Hospital, Program in Neuroscience, Harvard Medical School, Boston, MA 02115, USA

ARTICLE INFO

ABSTRACT

Mutations in PTEN-induced putative kinase 1 (PINK1) cause a recessive form of Parkinson's disease (PD). PINK1 is associated with mitochondrial quality control and its partial knock-down induces mitochondrial dysfunction including decreased membrane potential and increased vulnerability against mitochondrial toxins, but the exact function of PINK1 in mitochondria has not been investigated using cells with null expression of PINK1. Here, we show that loss of PINK1 caused mitochondrial dysfunction. In PINK1-deficient ($PINK1^{-/-}$) mouse embryonic fibroblasts (MEFs), mitochondrial membrane potential and cellular ATP levels were decreased compared with those in littermate wild-type MEFs. However, mitochondrial proton leak, which reduces membrane potential in the absence of ATP synthesis, was not altered by loss of PINK1. Instead, activity of the respiratory chain, which produces the membrane potential by oxidizing substrates using oxygen, declined. H_2O_2 production rate by $PINK1^{-/-}$ mitochondria was lower than $PINK1^{+/+}$ mitochondria as a consequence of decreased oxygen consumption rate, while the proportion (H_2O_2 production rate per oxygen consumption rate) was higher. These results suggest that mitochondrial dysfunctions in PD pathogenesis are caused not by proton leak, but by respiratory chain defects.

© 2010 Elsevier Inc. All rights reserved.

Introduction

Parkinson's disease (PD) is a neurodegenerative disease characterized by loss of dopaminergic neurons in the substantia nigra. Mitochondrial dysfunction has been proposed as a major factor in the pathogenesis of sporadic and familial PD (Abou-Sleiman et al., 2006). In particular, the identification of mutations in PTEN-induced putative kinase 1 (PINK1) has strongly implicated mitochondrial dysfunction owing to its loss of function in the pathogenesis of PD (Valente et al., 2004). PINK1 contains an N-terminal mitochondrial targeting sequence (MTS) and a serine/threonine kinase domain (Valente et al., 2004). PINK1 kinase activity is crucial for mitochondrial maintenance via TRAP

phosphorylation (Pridgeon et al., 2007). Loss of PINK1 function induces increased vulnerability to various stresses (Exner et al., 2007; Haque et al., 2008; Pridgeon et al., 2007; Wood-Kaczmar et al., 2008). However, silencing of PINK1 has only been partial and only one study has been performed to assess mitochondrial functions in steady and artificial states with complete ablation of PINK1 expression (Gautier et al., 2008).

Several studies have shown that PINK1 acts upstream of parkin in the same genetic pathway (Clark et al., 2006; Park et al., 2006) and co-overexpressed PINK1 and parkin both co-localized to mitochondria (Kim et al., 2008). Overexpression of PINK1 promotes mitochondrial fission (Yang et al., 2008). Fission followed by selective fusion segregates dysfunctional mitochondria and permits their removal by autophagy (Twig et al., 2008). PINK1 loss-of-function decreases mitochondrial membrane potential (Chu, 2010) and the PINK1-parkin pathway is associated with mitochondrial elimination in cultured cells treated with the mitochondrial uncoupler carbonyl cyanide m-chlorophenylhydrazone (CCCP), which causes mitochondrial depolarization (Geisler et al., 2010; Kawajiri et al., 2010; Matsuda et al., 2010; Narendra et al., 2008, 2010; Vives-Bauza et al., 2010). However, the exact mechanism underlying the mitochondrial depolarization induced by PINK1 defects leading to mitochondrial autophagy has not been examined in detail.

Here, we describe a detailed characterization of mitochondria in PINK1-deficient cells. We show that PINK1 deficiency causes a decrease in mitochondrial membrane potential, which is not due to proton leak, but to respiratory chain defects.

Materials and methods

PINK1 knock-out mouse embryonic fibroblasts (MEFs)

PINK1 knock-out MEFs were prepared and cultured as described previously (Matsuda et al., 2010). Mouse embryonic fibroblasts (MEFs) were derived from E12.5 embryos containing littermate 4 mice of each genotype. Embryos were mechanically dispersed by repeated passage through a P1000 pipette tip and plated with MEF media containing DME, 10% FCS, 1× nonessential amino acids, 1 mM L-glutamine, penicillin/streptomycin (invitrogen). The $\psi2$ cell line, an ecotropic retrovirus packaging cell line, was maintained in Dulbecco's modified Eagle medium (DMEM, Sigma) with 5% fetal bovine serum and 50 μg/ml kanamicin. Transfection of the $\psi2$ cells with pMESVTS plasmids containing an SV40 large T antigen was performed by lipofection method according to the manual provided by the manufacturer (GIBCO BRL). Five micrograms of the plasmids was used for each transfection. Transfectants were selected by G418 at the concentration of 0.5 mg/ml, and 10 clonal cell lines were established. The highest titer of 5×10^4 cfu/ml was obtained for the conditioned medium of a cell line designated $\psi2SVTS1$. 10^6 MEFs were plated onto a 10-cm culture dish and kept at 33 °C for 48 hours. Then medium was replaced with 2 ml supplemented with polybrene-supplemented medium conditioned by the $\psi2SVTS1$ cells at confluency for 3 days. Infection was continued for 3 hours, and the medium was replaced with a fresh one. The infected MEFs were cultured at 33 °C until immortalized cells were obtained.

We confirmed that the differences we detected in this study were due to the PINK1 deficiency, not to artificial effects by immortalization, by measuring cellular respiration rates of not immortalized MEFs from other littermates (Supplemental figure). The respiration rates of not immortalized MEFs were slightly slower than those of immortalized MEFs, but the differences between PINK1 $^{+/+}$ and $^{-/-}$ MEFs were consistent (Fig. 2A).

Cell growth

Cells were seeded in 12-well plates at density of $3 \sim 6 \times 10^3$ cells/well and incubated in DMEM high glucose medium (4.5 g/l glucose and 1 mM sodium pyruvate) supplemented with 10% fetal bovine serum. After a day, the medium was replaced with DMEM glucose-free medium supplemented with 1 g/l galactose, 1 mM sodium pyruvate and 10% fetal bovine serum (DMEM galactose medium) at 37 °C in an incubator with a humidified atmosphere of 5% CO₂. Cells were trypsinized and live cells were assessed by trypan blue dye exclusion.

Mitochondrial morphological changes

Cells were seeded in 6-well plates at 2.0×10^5/well and incubated in DMEM high glucose medium (4.5 g/l glucose and 1 mM sodium pyruvate) supplemented with 10% fetal bovine serum and 1% penicillin/streptomycin. After a day, the medium was replaced with DMEM glucose-free medium supplemented with 1 g/l galactose, 1 mM sodium pyruvate and 10% fetal bovine serum (DMEM galactose medium) at 37 °C in an incubator with a humidified atmosphere of 5% CO₂. 24 hours later, cells were fixed and immunostained with anti-Tom20 antibody to visualize mitochondria according to a protocol as previously described (Kawajiri et al., 2010). All images were obtained using an Axioplan 2 imaging microscope (Carl Zeiss, Oberkochen, Germany).

Cellular ATP levels

Intracellular ATP levels were determined by a cellular ATP assay kit (TOYO B-Net, Tokyo, Japan) according to the manufacturer's instructions using a Lumat LB9507 luminometer (Berthold Technology, Bad Wildbad, Germany).

Membrane potential

Fluorescence images were recorded using a multi-dimensional imaging workstation (AS MDW, Leica Microsystems, Wetzlar, Germany) with a climate chamber maintained at 37 °C. Fluorescence was quantified with a CCD camera (CoolSnap HQ, Roper Scientific, Princeton, NJ) using a 20× objective. Cells were stained for 1 hour with a non-quenching concentration (20 nM) of tetramethylrhodamine methyl ester (TMRM) in a 96-well plate. The cell-permeable cationic dye TMRM accumulates in mitochondria according to the Nernst equation. Nuclei were stained with 250 nM Hoechst 34580. Mitochondrial TMRM fluorescence was integrated in a 40-μm diameter circular area around the nucleus, and the minimum fluorescence in this area was subtracted as background fluorescence.

Cell respiration

Cell respiration was measured at 37 °C using the Oxygen Meter Model 781 and the Mitocell MT200 closed respiratory chamber (Strathkelvin Instruments, North Lanarkshire, United Kingdom). Cells were cultured in DMEM with 4.5 g/l of glucose supplemented with 10% FBS. Cells were then trypsinized and resuspended in Leibovitz's L-15 medium (Invitrogen) at density of 8.0×10^6 cells/ml. The oxygen respiration rate was measured under each of the following three conditions: basal rate (no additions); State 4 (no ATP synthesis) [after addition of 1 μg/ml oligomycin (Sigma)], uncoupled [after addition of 3 μM FCCP (carbonyl cyanide p-trifluoromethoxyphenylhydrazone; Sigma)] using Strathkelvin 949 Oxygen System. After sequential measurements, the endogenous respiration rate was determined by adding 1 μM rotenone + 2 μM myxothiazol.

Mitochondrial respiration and membrane potential

Mitochondria were prepared from cultured MEFs as previously described (Amo and Brand, 2007). Mitochondrial oxygen consumption with 5 mM succinate as a respiratory substrate was measured at 37 °C using a Clark electrode (Rank Brothers, Cambridge, United Kingdom) calibrated with air-saturated respiration buffer comprising 0.115 M KCl, 10 mM KH₂PO₄, 3 mM HEPES (pH 7.2), 2 mM MgCl₂, 1 mM EGTA and 0.3% (w/v) defatted BSA, assumed to contain 406 nmol atomic oxygen/ml (Reynafarje et al., 1985). Mitochondrial membrane potential ($\Delta\psi$) was measured simultaneously with respiratory activity using an electrode sensitive to the lipophilic cation TPMP$^+$ (triphenylmethylphosphonium) (Brand, 1995). Mitochondria were incubated at 0.5 mg/ml in the presence of 80 ng/ml nigericin (to collapse the pH gradient so that the proton motive force was expressed exclusively as $\Delta\psi$) and 2 μM rotenone (to inhibit complex I). The TPMP$^+$-sensitive electrode was calibrated with sequential additions of TPMP$^+$ up to 2 μM, then 5 mM succinate was added to initiate respiration. Experiments were terminated with 2 μM FCCP, allowing correction for any small baseline drift. $\Delta\psi$ was calculated from the distribution of TPMP$^+$ across the mitochondrial inner membrane using a binding correction factor of 0.35 mg protein/μl. Respiratory rates with 4 mM pyruvate + 1 mM malate as a substrate in State 3 (with 0.25 mM ADP) and State 4 (with 1 μg/ml oligomycin) were determined using the Oxygen Meter Model 781 and the Mitocell MT200 closed respiratory chamber (Strathkelvin Instruments).

Modular kinetic analysis

To investigate differences in oxidative phosphorylation caused by PINK1 knock-out, we applied a systems approach, namely modular kinetic analysis (Amo and Brand, 2007; Brand, 1990). This analyzes the kinetics of the whole of oxidative phosphorylation divided into three modules connected by their common substrate or product, $\Delta\psi$. The modules are (i) the reactions that produce $\Delta\psi$, consisting of the substrate translocases, dehydrogenases and other enzymes and the components of the respiratory chain, called 'substrate oxidation'; (ii) the reactions that consume $\Delta\psi$ and synthesize, export and dephosphorylate ATP, consisting of ATP synthase, the phosphate and adenine nucleotide translocases and any ATPases that may be present, called the 'phosphorylating system'; and (iii) the reactions that consume $\Delta\psi$ without ATP synthesis, called the 'proton leak' (Brand, 1990). The analysis reports changes anywhere within oxidative phosphorylation that are functionally important but is unresponsive to changes that have no functional consequences. Comparison of the kinetic responses of each of the three modules to $\Delta\psi$ obtained using mitochondria isolated from PINK1$^{+/+}$ and PINK1$^{-/-}$ MEFs would reveal any effects of PINK1 on the kinetics of oxidative phosphorylation. Oxygen consumption and $\Delta\psi$ were measured simultaneously using mitochondria incubated with 80 ng/ml nigericin and 4 μM rotenone. Respiration was initiated by 5 mM succinate. The kinetic behavior of a '$\Delta\psi$-producer' can be established by specific modulation of a $\Delta\psi$-consumer and the kinetics of a consumer can be established by specific modulation of a $\Delta\psi$-producer (Brand, 1998). To measure the kinetic response of proton leak to $\Delta\psi$, the State 4 (non-phosphorylating) respiration of mitochondria in the presence of oligomycin (0.8 μg/ml; to prevent any residual ATP synthesis), which was used solely to drive the proton leak, was titrated with malonate (up to 8 mM). In a similar way, State 4 respiration was titrated by FCCP (up to 1 μM) for measurement of the kinetic response of substrate oxidation to $\Delta\psi$. State 3 (maximal rate of ATP synthesis) was obtained by addition of excess ADP (1 mM). Titration of State 3 respiration with malonate (up to 1.1 mM) allowed measurement of the kinetics of the $\Delta\psi$-consumers (the sum of the phosphorylating system and proton leak). The coupling efficiencies of oxidative phosphorylation were calculated from the kinetic curves as the percentage of mitochondrial respiration rate at a given $\Delta\psi$ that was used for ATP synthesis and was therefore inhibited by oligomycin. Note that any slip reactions will appear as proton leak in this analysis (Brand et al., 1994).

Mitochondrial ROS production

Mitochondrial ROS production rate was assessed by measurement of H_2O_2 generation rate, determined fluorometrically by measurement of oxidation of Amplex Red to fluorescent resorufin coupled to the enzymatic reduction of H_2O_2 by horseradish peroxidase using a spectrofluorometer RF-5300PC (Shimadzu, Kyoto, Japan). The H_2O_2 generation rate was measured in non-phosphorylating conditions (= State 4) using either pyruvate/malate or succinate as respiratory substrates. Mitochondria were incubated at 0.1 mg/ml in respiration buffer. All incubations also contained 5 μM Amplex Red, 2 U/ml horseradish peroxidase and 8 U/ml superoxide dismutase. The reaction was initiated by addition of 5 mM succinate or 4 mM pyruvate + 1 mM malonate and the increase in fluorescence was followed at excitation and emission wavelengths of 560 and 590 nm, respectively. Appropriate correction for background signals and standard curves generated using known amounts of H_2O_2 were used to calculate the rate of H_2O_2 production in nmol/min/mg mitochondrial protein. The percentage free radical leak, which is a measure of the number of electrons that produce superoxide (and subsequently H_2O_2) compared with the total number of electrons which pass thorough the respiratory chain, was calculated as the rate of H_2O_2 production divided by the rate of O_2 consumption (Barja et al., 1994).

Statistics

Values are presented as means ± SEM except Fig. 2D, in which error bars indicate SD. The significance of differences between means was assessed by the unpaired Student's *t*-test using Microsoft Excel; *P* values < 0.05 were taken to be significant.

Results

Cell growth and mitochondrial morphology

In general, cultured cells gain their energy mostly from glycolysis. Therefore, cells deficient in respiratory function can grow in normal medium, although possibly at a slower rate, relying predominantly on glycolysis (Hofhaus et al., 1996). Actually, ρ^0 cells, which lack mitochondrial DNA completely, can grow producing energy exclusively through glycolysis (King and Attardi, 1989). On the other hand, galactose metabolism via glycolysis is much slower than glucose metabolism (Reitzer et al., 1979). Therefore, cells in galactose medium are forced to oxidize pyruvate through the mitochondrial respiratory chain for energy required for growth. Consequently, cells with defects in their mitochondrial respiratory chains show growth impairments in galactose medium. To evaluate this phenomenon is also observed in our cells, we examined growth retardation by addition of mitochondrial complex I inhibitor, rotenone (Fig. 1A). In glucose medium, 10 nM rotenone had only a slight effect on the growth of PINK1$^{+/+}$ MEFs and slower growth was observed even in the presence of 100 nM rotenone. However, in the galactose medium, 10 nM rotenone significantly inhibited the growth of PINK1$^{+/+}$ MEFs and 100 nM roteone completely arrested the growth. Therefore, we could confirm that the growth impairment of our cells in the galactose medium was due to mitochondrial respiratory chain defects.

PINK1 acts upstream of parkin, regulating mitochondrial integrity and function; therefore, loss of PINK1 is considered to affect mitochondrial functions. To assess the mitochondrial functions of PINK1$^{-/-}$ MEFs, growth capability in a medium in which galactose replaced glucose was examined. As shown in Fig. 1B, PINK1$^{-/-}$ MEFs appeared to show clear growth impairments in the galactose medium, whereas PINK1$^{+/+}$ MEFs grew slightly slower than in the glucose medium.

No differences of mitochondrial morphology between PINK1$^{+/+}$ and $^{-/-}$ MEFs in the glucose medium were detected (Fig. 1C), consistent with the previous report (Matsuda et al., 2010). However, in the galactose medium, mitochondria of the PINK1$^{-/-}$ MEFs were more fragmented compared to the PINK$^{+/+}$ MEFs (Fig. 1C). This is consistent with previous reports, which found mitochondrial morphological changes were more pronounced when PINK1 knock-down HeLa cells were grown in low-glucose medium (Exner et al., 2007) and human PINK1 homozygous mutant fibroblast in galactose medium (Grünewald et al., 2009). In these cells, mitochondrial morphological changes were associated with the mitochondrial functional impairment.

Assessments of mitochondrial functions at the cellular level

Because PINK1$^{-/-}$ MEFs showed severe growth impairments in the galactose medium, the mitochondrial functions of these cells were assessed at the cellular level. First, cellular respiration rates were measured (Fig. 2A). The basal respiration rate was significantly reduced in PINK1$^{-/-}$ cells compared with that in PINK1$^{+/+}$ cells (11.13 ± 0.71 versus 14.36 ± 1.01 nmol O/min/10^6 cells; $p < 0.05$; $n = 5$ independent experiments), consistent with previous reports using partial knock-down of PINK1 expression (Gandhi et al., 2009; Liu et al., 2009). Oligomycin inhibits ATP synthase, resulting in non-phosphorylating respiration. FCCP uncouples oxidative phosphorylation, leading to maximum respiration rates. In both conditions, the
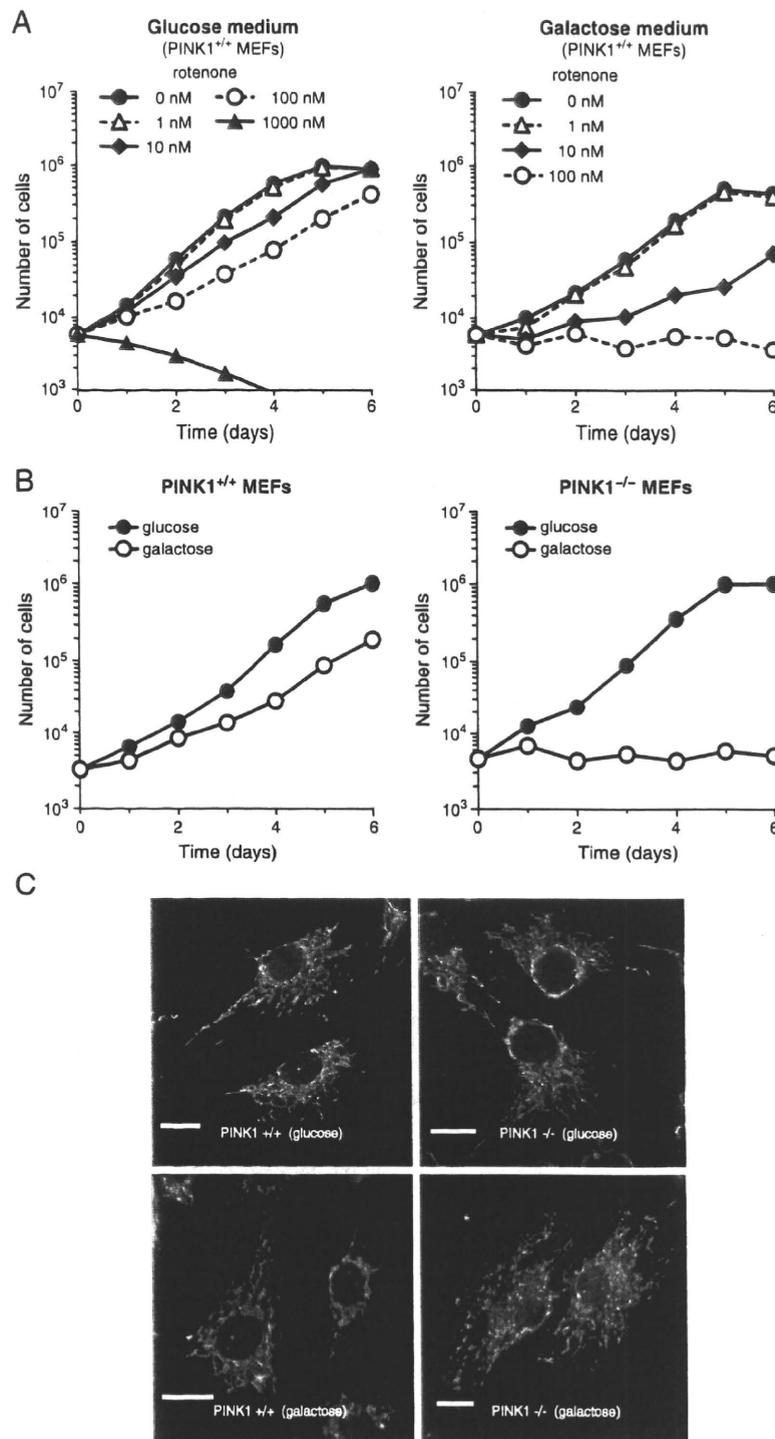
Fig. 1. (A) Growth retardation of PINK1 $^{+/+}$ MEFs by mitochondrial complex I inhibitor, rotenone in glucose or galactose medium. Closed circles with solid line, 0 nM rotenone; open triangles with dashed line, 1 nM rotenone; closed diamonds with solid line, 10 nM rotenone; open circles with dashed line, 100 nM rotenone; closed triangles with solid line, 1000 nM rotenone. Cells grown in 12-well plates were trypsinized and live cells were assessed by trypan blue dye exclusion. (B) Growth curves of PINK1 $^{+/+}$ and $^{-/-}$ MEFs. Closed symbols (*glucose*), growth curve for cells grown in DMEM containing 4.5 g/l glucose and 1 mM sodium pyruvate; open symbols (*galactose*), growth curve for cells grown in DMEM lacking glucose and containing instead 1.0 g/l galactose and 1 mM sodium pyruvate. Cells grown in 12-well plates were trypsinized and live cells were assessed by trypan blue dye exclusion. (C) Mitochondrial morphology of PINK1 $^{+/+}$ and $^{-/-}$ MEFs. After incubating cells with the glucose or galactose medium for 24 hours, cells were fixed and immunostained with anti-Tom20 antibody to visualize mitochondria. Scale bar, 20 μm.

PINK1 $^{-/-}$ cells respired significantly slower than the PINK1 $^{+/+}$ cells (1.76 ± 0.13 versus 2.95 ± 0.27 ($p < 0.01$; $n = 5$ independent experiments) and 16.44 ± 1.80 versus 23.50 ± 1.18 nmol O/min/10^6 cells ($p < 0.05$; $n = 5$ independent experiments), respectively).

The main function of mitochondria is ATP synthesis via oxidative phosphorylation. ATP levels under basal conditions were significantly reduced in PINK1 $^{-/-}$ MEFs (Fig. 2B), as reported previously for dissociated PINK1 $^{-/-}$ mouse neurons (Gispert et al., 2009) and PINK1
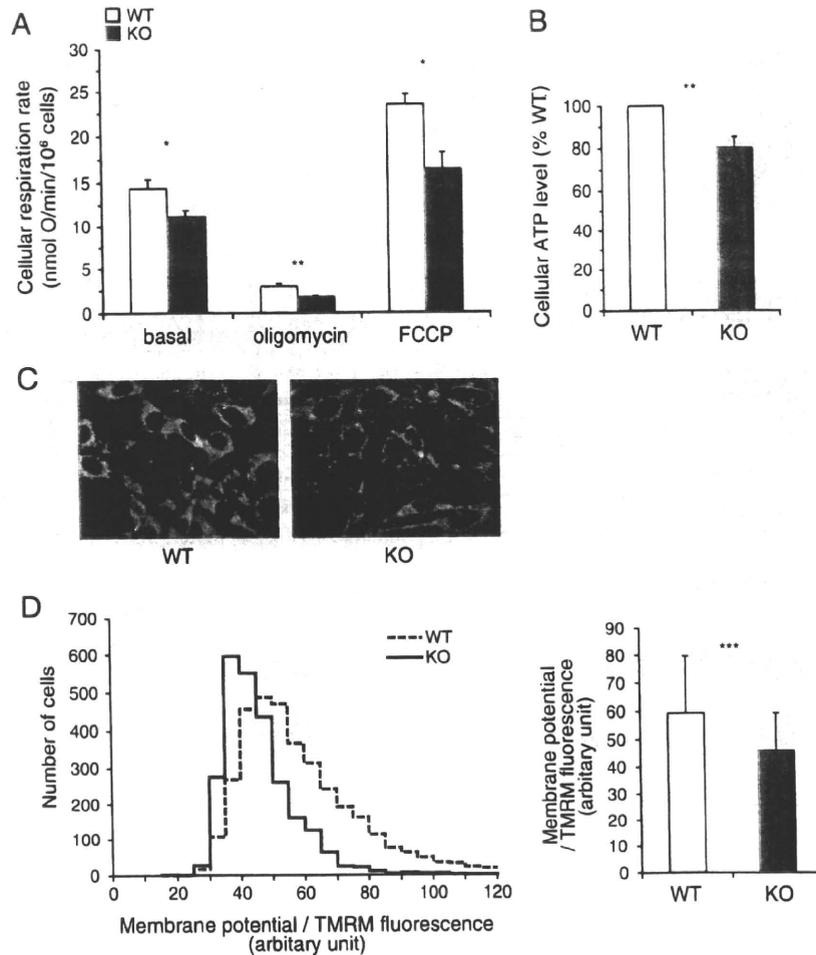
Fig. 2. Mitochondrial functions assessed at the cellular level. Open bars, PINK1$^{+/+}$ MEFs; closed bars, PINK1$^{-/-}$ MEFs. (A) Cell respiration rate of PINK1$^{+/+}$ and $^{-/-}$ MEFs. The oxygen respiration rate was measured at density of 8.0×10^6 cells/ml under each of the following three conditions: basal rate (no additions); State 4 (no ATP synthesis) [after addition of 1 µg/ml oligomycin], uncoupled [after addition of 3 µM FCCP]. After sequential measurements, the endogenous respiration rate was determined by adding 1 µM rotenone + 2 µM myxothiazol. Error bars indicate SEM ($n = 5$ independent experiments). (B) Cellular ATP levels. Data were normalized based on cell numbers and expressed as the percentage of the level in PINK1$^{+/+}$ cells. Error bars indicate SEM ($n = 4$ independent experiments). (C) Live cell images of PINK1$^{+/+}$ and $^{-/-}$ MEFs with TMRM fluorescence. (D) Mitochondrial membrane potential evaluated by live cell imaging of TMRM fluorescence. Left panel, the distribution of TMRM fluorescence from 3537 PINK1$^{+/+}$ and 2566 PINK1$^{-/-}$ cells from 12 wells per cell type; right panel, the average value of TMRM fluorescence per cell. Error bars indicate SD. *$P<0.05$; **$P<0.01$; ***$P<0.001$.

siRNA knock-down PC12 cells (Liu et al., 2009). Mitochondrial membrane potential was also measured by live cell imaging of TMRM fluorescence. Typical images were shown in Fig. 2C. The histogram shows the distribution of TMRM fluorescence from 3537 PINK1$^{+/+}$ cells and 2566 PINK1$^{-/-}$ cells from 12 wells per cell type and the bar graph indicates the mean ± SD of TMRM fluorescence per cell (Fig. 2D). According to the Nernst equation, the ratio of TMRM fluorescence would translate into, on average, 6.88 mV lower mitochondrial membrane potential in the PINK1$^{-/-}$ cells if the plasma membrane potentials were not different between PINK1$^{+/+}$ and $^{-/-}$ cells. Mitochondrial membrane potential decrease was also showed previously in PINK1 knock-down HeLa cells (Exner et al., 2007) and in stable PINK1 knock-down neuroblastoma cell lines (Sandebring et al., 2009).

Assessments of mitochondrial functions using isolated mitochondria

To further analyze mitochondrial functions, we measured the kinetics of oxidative phosphorylation using isolated mitochondria from PINK1$^{+/+}$ and $^{-/-}$ MEFs. Fig. 3 shows the kinetics of the three modules of oxidative phosphorylation using succinate as a respiratory substrate (complex II-linked respiration). Fig. 3A shows the kinetic response of substrate oxidation to its product, Δψ. The

substrate oxidation kinetic curve for PINK1$^{-/-}$ cells was clearly shifted lower compared with that for PINK1$^{+/+}$ cells, indicating that the loss of PINK1 caused mitochondrial respiratory chain defects. Fig. 3B shows the kinetic response of proton leak to its driving force, Δψ, and Fig. 3C shows the kinetic response of the ATP phosphorylating pathway to its driving force, Δψ. Both kinetic curves for PINK1$^{+/+}$ and $^{-/-}$ MEFs (open and closed symbols, respectively) were overlapping, implying that there were no significant differences in those modules.

We also independently measured the mitochondrial oxygen consumption rate using pyruvate/malate as a respiratory substrate instead of succinate to check complex I. Modular kinetic analysis using pyruvate/malate is technically difficult for the following reasons: (1) the oxygen consumption rate with pyruvate/malate is much slower than succinate respiration; and (2) there are no competitive inhibitors of complex I-linked respiration, such as malonate for succinate respiration. As shown in Fig. 4A, the respiration rates in State 3 and 4 with pyruvate/malate of isolated mitochondria from PINK1$^{-/-}$ cells (closed symbols) were significantly slower than those of PINK1$^{+/+}$ cells (open symbols), as in the case of succinate respiration (Fig. 4B; data derived from the kinetic curves in Fig. 3).
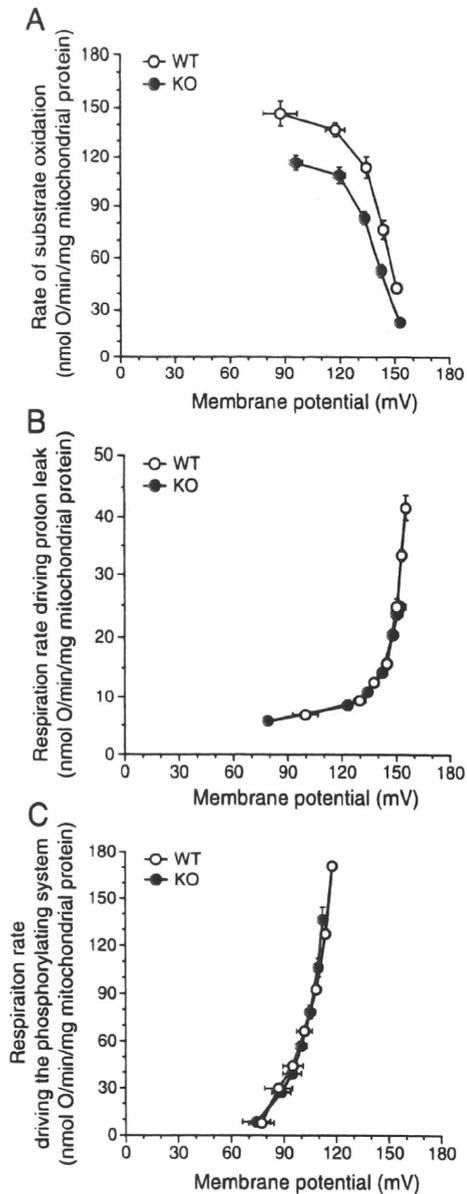
Fig. 3. Modular kinetic analysis of oxidative phosphorylation in mitochondria isolated from PINK1$^{+/+}$ and $^{-/-}$ MEFs. Modular kinetic analysis of the kinetic responses to membrane potential, $\Delta\psi$, of respiration driving (A) substrate oxidation ($\Delta\psi$ titrated with uncoupler, FCCP, starting in State 4), (B) proton leak ($\Delta\psi$ titrated with malonate, starting in State 4) and (C) the phosphorylating system, calculated by subtracting respiration driving proton leak from respiration driving the $\Delta\psi$-consumers ($\Delta\psi$ titrated with malonate starting in State 3; not shown) at each $\Delta\psi$. Open symbols, PINK1$^{+/+}$ MEFs; closed symbols, PINK1$^{-/-}$ MEFs. Error bars indicate SEM ($n = 4$ independent mitochondrial preparations).

Mitochondrial ROS production

Mitochondrial ROS production rate was assessed by measurement of the H$_2$O$_2$ generation rate. Mechanisms of mitochondrial ROS production were well described elsewhere (Fig. 1 of Lambert et al., 2010). Pyruvate and malate generate NADH, which induced forward electron transport and generate ROS mainly from complex I and III. For pyruvate/malate respiration, the basal H$_2$O$_2$ generation rate (measured in the absence of respiratory chain inhibitors) was not different between PINK1$^{+/+}$ and $^{-/-}$ mitochondria (Fig. 4C). The addition of antimycin A and further addition of rotenone, which inhibited forward electron transport at complex III and I, respectively,

enhanced H$_2$O$_2$ generation. During succinate respiration in the absence of respiratory chain inhibitors, ROS are generated mainly from the quinine binding site of complex I due to reverse electron flow from coenzyme Q to complex I. For succinate respiration, H$_2$O$_2$ generation rate in the absence of reparatory chain inhibitors was higher in PINK1$^{+/+}$ mitochondria than in PINK1$^{-/-}$ mitochondria, but the difference was not significant (Fig. 4D). The addition of rotenone, which blocks reverse electron flow from coenzyme Q to complex I, attenuated H$_2$O$_2$ generation.

Figs. 4 C and D show a tendency for PINK1$^{+/+}$ mitochondria to generate more ROS than PINK1$^{-/-}$ mitochondria. However, their respiration rates were remarkably different (Figs. 4A and B). Therefore, we calculated the percentage free radical leak, which is the fraction of molecules of O$_2$ consumed that give rise to H$_2$O$_2$ release by mitochondria (free radical leak) during either pyruvate/malate or succinate State 4 respiration (Figs. 4E and F). For pyruvate/malate respiration, mitochondria isolated from PINK1$^{-/-}$ cells had higher proportion of H$_2$O$_2$ generation than PINK1$^{+/+}$ mitochondria. During succinate respiration without respiratory inhibitors, PINK1$^{-/-}$ mitochondria had also higher proportion of free radical leak mainly from complex I due to reverse electron flow from coenzyme Q to complex I. Because the differences disappeared with addition of rotenone, which inhibit reverse electron flow, ROS generation enhanced by loss of PINK1 was mostly from complex I.

Discussion

We produced an *in vitro* model of Parkinson's disease, immortalized PINK1$^{-/-}$ MEFs. Previously, impairment of mitochondrial respiration was observed in the brains of PINK1$^{-/-}$ mice (Gautier et al., 2008). PINK1$^{-/-}$ MEFs clearly showed a phenotype of mitochondrial dysfunctions, which is consistent with PD pathogenesis. This phenotype was apparent in a cell growth experiment using medium containing galactose instead of glucose (Fig. 1B). Mitochondrial fragmentation was observed when PINK1$^{-/-}$ MEFs grew in the galactose medium (Fig. 1C), which was consistent with previous reports (Exner et al., 2007; Grünewald et al., 2009). Our results have unveiled that the PINK1$^{-/-}$ MEF line could be a potential PD model, presenting growth retardation due to decreased mitochondrial respiration activity. Thus, the PINK1$^{-/-}$ MEFs are a useful tool for evaluating the role of PINK1 in mitochondrial dysfunction and relevant to PD.

In PINK1$^{-/-}$ MEFs, mitochondrial membrane potential was decreased compared with that in littermate wild-type MEFs (Figs. 2C and D), as reported previously for PINK1 knock-down HeLa cells (Exner et al., 2007) and stable PINK1 knock-down neuroblastoma cell lines (Sandebring et al., 2009). This is a key event during elimination of mitochondria. Mitochondrial fission followed by selective fusion segregates damaged mitochondria, which decreases their membrane potential, and permits their removal by autophagy (Twig et al., 2008). The PINK1-parkin pathway is thought to have a crucial role in this mitochondrial elimination mechanism (Geisler et al., 2010; Kawajiri et al., 2010; Matsuda et al., 2010; Narendra et al., 2008, 2010; Vives-Bauza et al., 2010). To clarify what caused the decrease in mitochondrial membrane potential, we performed a modular kinetic analysis using isolated mitochondria (Fig. 3). This analyzes the kinetics of the whole of oxidative phosphorylation divided into three modules connected by their common substrate or product, mitochondrial membrane potential ($\Delta\psi$). The modules are include one $\Delta\psi$-producer (substrate oxidation) and two $\Delta\psi$-consumers (phosphorylating system and proton leak) (Brand, 1990). To decrease $\Delta\psi$, the $\Delta\psi$-producer should be down-regulated and/or $\Delta\psi$-consumers should be up-regulated. As cellular ATP levels were decreased compared with those in littermate wild-type MEFs (Fig. 2B), it is unlikely that the phosphorylating system is up-regulated. Indeed, the kinetics of the phosphorylation module were not altered (Fig. 3C). The other $\Delta\psi$-consumer, proton leak,
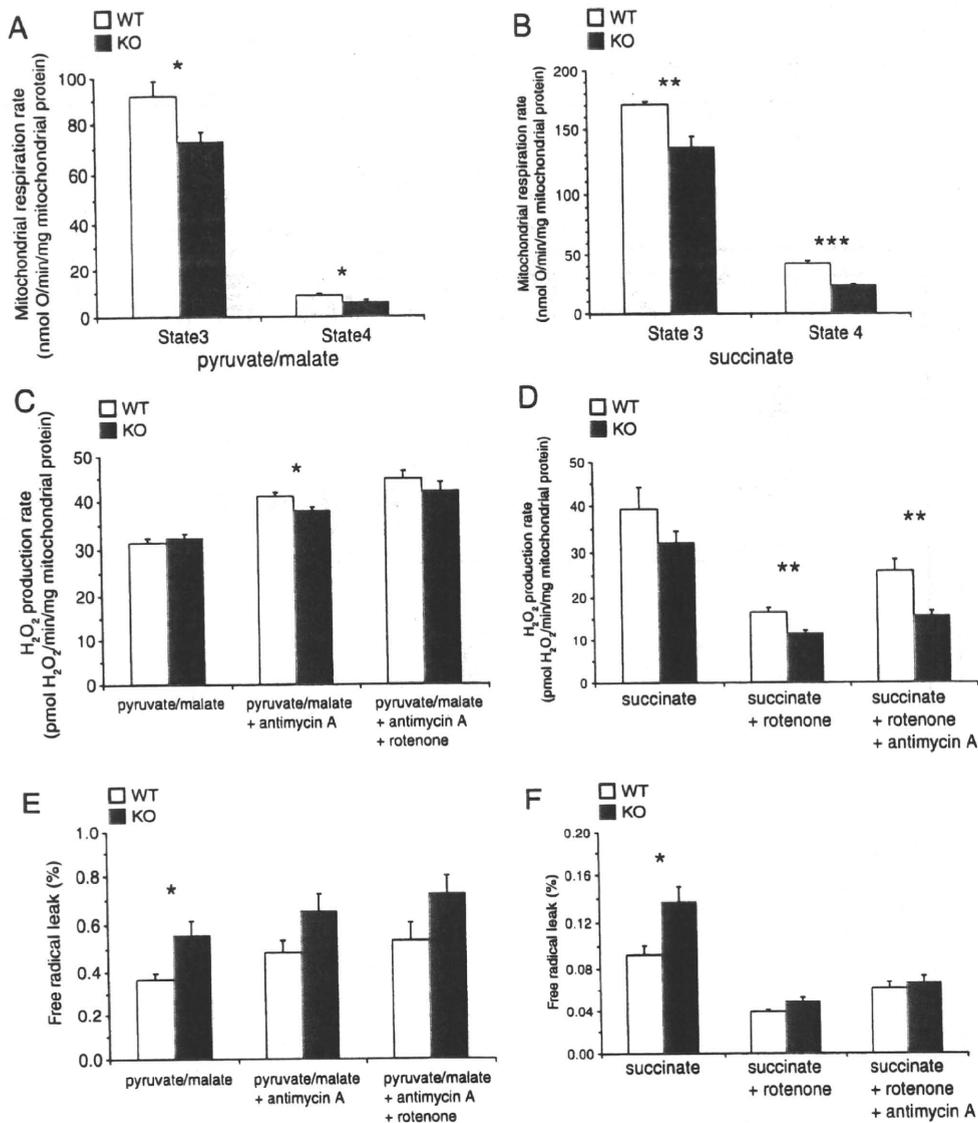
Fig. 4. Oxygen consumption rate and H₂O₂ production rate of mitochondria isolated from PINK1 [+/+] and [−/−] MEFs. Open bars, PINK1 [+/+] MEFs; closed bars, PINK1 [−/−] MEFs. (A) State 3 and State 4 respiration rate of mitochondria with pyruvate/malate as a respiratory substrate. (B) State 3 and State 4 respiration rate of mitochondria with succinate as a respiratory substrate. Data were derived from the results of modular kinetic analysis (Fig. 3). State 3 respiration rates were the kinetic start points of the Δψ-consumers (the sum of the phosphorylating system and proton leak). State 4 respiration rates were average values of the respiration rates at the kinetic start points of substrate oxidation and proton leak. (C, D) Mitochondrial H₂O₂ production rate with pyruvate/malate (C) or succinate (D) as a respiratory substrate. (E, F) Percentage free radical leak (FRL) for State 4 respiration with pyruvate/malate (E) or succinate (F) as a respiratory substrate. Error bars indicate SEM ($n = 5$ and 4 independent mitochondrial preparations for pyruvate/malate and succinate respiration, respectively). *$P<0.05$; **$P<0.01$; ***$P<0.001$.

which partially dissipates the membrane potential without ATP synthesis, was also not changed (Fig. 3B). Therefore, the decrease in membrane potential caused by loss of PINK1 is likely to have been caused only by lower activity of the Δψ-producer, substrate oxidation (Fig. 3A). This is the first report showing that mitochondrial membrane potential decrease caused by loss of PINK1, which is the key event for the following mitochondrial elimination, was not due to proton leak, but to respiratory chain defects. We used only succinate (a complex II-linked substrate) as a respiratory substrate in the modular kinetic analysis for technical reasons. However, complex I-linked respiration (pyruvate/malate) was also decreased in PINK1 [−/−] MEFs like succinate respiration (Fig. 4A).

The mitochondrial respiration rates in State 4 were decreased in PINK1 [−/−] MEFs, and consequently, the proportions of free radical leak were significantly higher in PINK1 [−/−] MEFs than in PINK1 [+/+]

MEFs (Figs. 4E and F). Because the differences disappeared with addition of rotenone (complex I inhibitor, which inhibits reverse electron flow from coenzyme Q to complex I), ROS generation enhanced by loss of PINK1 was mostly from complex I. These results are partially consistent with those in previous reports, suggesting that MPTP and rotenone induce neuronal cell death by inhibiting complex I activity, leading to a PD-like phenotype (Dauer and Przedborski, 2003; Jackson-Lewis and Przedborski, 2007; Troja-nowski, 2003).

In this study, we developed an *in vitro* PD model, the PINK1 [−/−] MEF line, and established the experimental conditions for cell growth to detect mitochondrial dysfunction. This is the first report showing that complete ablation of PINK1 causes a decrease in mitochondrial membrane potential, which is not due to proton leak, but to respiratory chain defects.

Supplementary materials related to this article can be found online at doi:10.1016/j.nbd.2010.08.027.

References

Abou-Sleiman, P.M., Muqit, M.M., Wood, N.W., 2006. Expanding insights of mitochondrial dysfunction in Parkinson's disease. Nat. Rev. Neurosci. 7, 207–219.

Amo, T., Brand, M.D., 2007. Were inefficient mitochondrial haplogroups selected during migrations of modern humans? A test using modular kinetic analysis of coupling in mitochondria from cybrid cell lines. Biochem. J. 404, 345–351.

Barja, G., Cadenas, S., Rojas, C., Pérez-Campo, R., López-Torres, M., 1994. Low mitochondrial free radical production per unit O_2 consumption can explain the simultaneous presence of high longevity and high aerobic metabolic rate in birds. Free Radic. Res. 21, 317–327.

Brand, M.D., 1990. The proton leak across the mitochondrial inner membrane. Biochim. Biophys. Acta 1018, 128–133.

Brand, M.D., 1995. Measurement of mitochondrial protonmotive force. In: Brown, G.C., Cooper, C.E. (Eds.), Bioenergetics, a practical approach. IRL Press, Oxford, pp. 39–62.

Brand, M.D., 1998. Top-down elasticity analysis and its application to energy metabolism in isolated mitochondria and intact cells. Mol. Cell. Biochem. 184, 13–20.

Brand, M.D., Chien, L.F., Diolez, P., 1994. Experimental discrimination between proton leak and redox slip during mitochondrial electron transport. Biochem. J. 297, 27–29.

Chu, C.T., 2010. Tickled PINK1: mitochondrial homeostasis and autophagy in recessive Parkinsonism. Biochim. Biophys. Acta 1802, 20–28.

Clark, I.E., Dodson, M.W., Jiang, C., Cao, J.H., Huh, J.R., Seol, J.H., Yoo, S.J., Hay, B.A., Guo, M., 2006. *Drosophila pink1* is required for mitochondrial function and interacts genetically with *parkin*. Nature 441, 1162–1166.

Dauer, W., Przedborski, S., 2003. Parkinson's disease: mechanisms and models. Neuron 39, 889–909.

Exner, N., Treske, B., Paquet, D., Holmstrom, K., Schiesling, C., Gispert, S., Carballo-Carbajal, I., Berg, D., Hoepken, H.H., Gasser, T., Krüger, R., Winklhofer, K.F., Vogel, F., Reichert, A.S., Auburger, G., Kahle, P.J., Schmid, B., Haass, C., 2007. Loss-of-function of human PINK1 results in mitochondrial pathology and can be rescued by parkin. J. Neurosci. 27, 12413–12418.

Gandhi, S., Wood-Kaczmar, A., Yao, Z., Plun-Favreau, H., Deas, E., Klupsch, K., Downward, J., Latchman, D.S., Tabrizi, S.J., Wood, N.W., Duchen, M.R., Abramov, A.Y., 2009. PINK1-associated Parkinson's disease is caused by neuronal vulnerability to calcium-induced cell death. Mol. Cell 33, 627–638.

Gautier, C.A., Kitada, T., Shen, J., 2008. Loss of PINK1 causes mitochondrial functional defects and increased sensitivity to oxidative stress. Proc. Natl. Acad. Sci. U. S. A. 105, 11364–11369.

Geisler, S., Holmström, K.M., Skujat, D., Fiesel, F.C., Rothfuss, O.C., Kahle, P.J., Springer, W., 2010. PINK1/Parkin-mediated mitophagy is dependent on VDAC1 and p62/SQSTM1. Nat. Cell Biol. 12, 119–131.

Gispert, S., Ricciardi, F., Kurz, A., Azizov, M., Hoepken, H.H., Becker, D., Voos, W., Leuner, K., Müller, W.E., Kudin, A.P., Kunz, W.S., Zimmermann, A., Roeper, J., Wenzel, D., Jendrach, M., García-Arencíbia, M., Fernández-Ruiz, J., Huber, L., Rohrer, H., Barrera, M., Reichert, A.S., Rüb, U., Chen, A., Nussbaum, R.L., Auburger, G., 2009. Parkinson phenotype in aged PINK1-deficient mice is accompanied by progressive mitochondrial dysfunction in absence of neurodegeneration. PLoS One 4, e5777.

Grünewald, A., Gegg, M.E., Taanman, J.W., King, R.H., Kock, N., Klein, C., Schapira, A.H., 2009. Differential effects of PINK1 nonsense and missense mutations on mitochondrial function and morphology. Exp. Neurol. 219, 266–273.

Haque, M.E., Thomas, K.J., D'Souza, C., Callaghan, S., Kitada, T., Slack, R.S., Fraser, P., Cookson, M.R., Tandon, A., Park, D.S., 2008. Cytoplasmic Pink1 activity protects

neurons from dopaminergic neurotoxin MPTP. Proc. Natl. Acad. Sci. U. S. A. 105, 1716–1721.

Hofhaus, G., Johns, D.R., Hurko, O., Attardi, G., Chomyn, A., 1996. Respiration and growth defects in transmitochondrial cell lines carrying the 11778 mutation associated with Leber's hereditary optic neuropathy. J. Biol. Chem. 271, 13155–13161.

Jackson-Lewis, V., Przedborski, S., 2007. Protocol for the MPTP mouse model of Parkinson's disease. Nat. Protoc. 2, 141–151.

Kawajiri, S., Saiki, S., Sato, S., Sato, F., Hatano, T., Eguchi, H., Hattori, N., 2010. PINK1 is recruited to mitochondria with parkin and associates with LC3 in mitophagy. FEBS Lett. 584, 1073–1079.

Kim, Y., Park, J., Kim, S., Song, S., Kwon, S.K., Lee, S.H., Kitada, T., Kim, J.M., Chung, J., 2008. PINK1 controls mitochondrial localization of Parkin through direct phosphorylation. Biochem. Biophys. Res. Commun. 377, 975–980.

King, M.P., Attardi, G., 1989. Human cells lacking mtDNA: repopulation with exogenous mitochondria by complementation. Science 246, 500–503.

Lambert, A.J., Buckingham, J.A., Boysen, H.M., Brand, M.D., 2010. Low complex I content explains the low hydrogen peroxide production rate of heart mitochondria from the long-lived pigeon, Columba livia. Aging Cell 9, 78–91.

Liu, W., Vives-Bauza, C., Acin-Perez, R., Yamamoto, A., Tan, Y., Li, Y., Magrane, J., Stavarache, M.A., Shaffer, S., Chang, S., Kaplitt, M.G., Huang, X.Y., Beal, M.F., Manfredi, G., Li, C., 2009. PINK1 defect causes mitochondrial dysfunction, proteasomal deficit and alpha-synuclein aggregation in cell culture models of Parkinson's disease. PLoS One 4, e4597.

Matsuda, N., Sato, S., Shiba, K., Okatsu, K., Saisho, K., Gautier, C.A., Sou, Y.S., Saiki, S., Kawajiri, S., Sato, F., Kimura, M., Komatsu, M., Hattori, N., Tanaka, K., 2010. PINK1 stabilized by mitochondrial depolarization recruits Parkin to damaged mitochondria and activates latent Parkin for mitophagy. J. Cell Biol. 189, 211–221.

Narendra, D., Tanaka, A., Suen, D.F., Youle, R.J., 2008. Parkin is recruited selectively to impaired mitochondria and promotes their autophagy. J. Cell Biol. 183, 795–803.

Narendra, D.P., Jin, S.M., Tanaka, A., Suen, D.F., Gautier, C.A., Shen, J., Cookson, M.R., Youle, R.J., 2010. PINK1 is selectively stabilized on impaired mitochondria to activate Parkin. PLoS Biol. 8, e1000298.

Park, J., Lee, S.B., Lee, S., Kim, Y., Song, S., Kim, S., Bae, E., Kim, J., Shong, M., Kim, J.M., Chung, J., 2006. Mitochondrial dysfunction in *Drosophila PINK1* mutants is complemented by *parkin*. Nature 441, 1157–1161.

Pridgeon, J.W., Olzmann, J.A., Chin, L.S., Li, L., 2007. PINK1 protects against oxidative stress by phosphorylating mitochondrial chaperone TRAP1. PLoS Biol. 5, e172.

Reitzer, L.J., Wice, B.M., Kennell, D., 1979. Evidence that glutamine, not sugar, is the major energy source for cultured HeLa cells. J. Biol. Chem. 254, 2669–2676.

Reynafarje, B., Costa, L.E., Lehninger, A.L., 1985. O_2 solubility in aqueous media determined by a kinetic method. Anal. Biochem. 145, 406–418.

Sandebring, A., Thomas, K.J., Beilina, A., van der Brug, M., Cleland, M.M., Ahmad, R., Miller, D.W., Zambrano, I., Cowburn, R.F., Behbahani, H., Cedazo-Mínguez, A., Cookson, M.R., 2009. Mitochondrial alterations in PINK1 deficient cells are influenced by calcineurin-dependent dephosphorylation of dynamin-related protein 1. PLoS One 4, e5701.

Trojanowski, J.Q., 2003. Rotenone neurotoxicity: a new window on environmental causes of Parkinson's disease and related brain amyloidoses. Exp. Neurol. 179, 6–8.

Twig, G., Elorza, A., Molina, A.J., Mohamed, H., Wikstrom, J.D., Walzer, G., Stiles, L., Haigh, S.E., Katz, S., Las, G., Alroy, J., Wu, M., Py, B.F., Yuan, J., Deeney, J.T., Corkey, B. E., Shirihai, O.S., 2008. Fission and selective fusion govern mitochondrial segregation and elimination by autophagy. EMBO J. 27, 433–446.

Valente, E.M., Abou-Sleiman, P.M., Caputo, V., Muqit, M.M., Harvey, K., Gispert, S., Ali, Z., Del Turco, D., Bentivoglio, A.R., Healy, D.G., Albanese, A., Nussbaum, R., González-Maldonado, R., Deller, T., Salvi, S., Cortelli, P., Gilks, W.P., Latchman, D.S., Harvey, R.J., Dallapiccola, B., Auburger, G., Wood, N.W., 2004. Hereditary early-onset Parkinson's disease caused by mutations in *PINK1*. Science 304, 1158–1160.

Vives-Bauza, C., Zhou, C., Huang, Y., Cui, M., de Vries, R.L., Kim, J., May, J., Tocilescu, M.A., Liu, W., Ko, H.S., Magrane, J., Moore, D.J., Dawson, V.L., Grailhe, R., Dawson, T.M., Li, C., Tieu, K., Przedborski, S., 2010. PINK1-dependent recruitment of Parkin to mitochondria in mitophagy. Proc. Natl. Acad. Sci. U. S. A. 107, 378–383.

Wood-Kaczmar, A., Gandhi, S., Yao, Z., Abramov, A.Y., Miljan, E.A., Keen, G., Stanyer, L., Hargreaves, I., Klupsch, K., Deas, E., Downward, J., Mansfield, L., Jat, P., Taylor, J., Heales, S., Duchen, M.R., Latchman, D., Tabrizi, S.J., Wood, N.W., 2008. PINK1 is necessary for long term survival and mitochondrial function in human dopaminergic neurons. PLoS One 3, e2455.

Yang, Y., Ouyang, Y., Yang, L., Beal, M.F., McQuibban, A., Vogel, H., Lu, B., 2008. Pink1 regulates mitochondrial dynamics through interaction with the fission/fusion machinery. Proc. Natl. Acad. Sci. U. S. A. 105, 7070–7075.

Molecular Hydrogen Improves Obesity and Diabetes by Inducing Hepatic FGF21 and Stimulating Energy Metabolism in *db/db* Mice

Naomi Kamimura[1], Kiyomi Nishimaki[1], Ikuroh Ohsawa[1,2] and Shigeo Ohta[1]

Recent extensive studies have revealed that molecular hydrogen (H_2) has great potential for improving oxidative stress-related diseases by inhaling H_2 gas, injecting saline with dissolved H_2, or drinking water with dissolved H_2 (H_2-water); however, little is known about the dynamic movement of H_2 in a body. First, we show that hepatic glycogen accumulates H_2 after oral administration of H_2-water, explaining why consumption of even a small amount of H_2 over a short span time efficiently improves various disease models. This finding was supported by an *in vitro* experiment in which glycogen solution maintained H_2. Next, we examined the benefit of *ad libitum* drinking H_2-water to type 2 diabetes using *db/db* obesity model mice lacking the functional leptin receptor. Drinking H_2-water reduced hepatic oxidative stress, and significantly alleviated fatty liver in *db/db* mice as well as high fat-diet-induced fatty liver in wild-type mice. Long-term drinking H_2-water significantly controlled fat and body weights, despite no increase in consumption of diet and water. Moreover, drinking H_2-water decreased levels of plasma glucose, insulin, and triglyceride, the effect of which on hyperglycemia was similar to diet restriction. To examine how drinking H_2-water improves obesity and metabolic parameters at the molecular level, we examined gene-expression profiles, and found enhanced expression of a hepatic hormone, fibroblast growth factor 21 (FGF21), which functions to enhance fatty acid and glucose expenditure. Indeed, H_2 stimulated energy metabolism as measured by oxygen consumption. The present results suggest the potential benefit of H_2 in improving obesity, diabetes, and metabolic syndrome.

INTRODUCTION

Oxidative stress is involved in many lifestyle-related diseases, including diabetes, atherosclerosis, heart failure, Alzheimer's disease, and Parkinson diseases (1–6). Recent studies have revealed that molecular hydrogen (H_2) acts as a novel antioxidant and prevents or ameliorates diseases associated with oxidative stress in animal experiments (7–18) and clinical tests (19–22). The brain, heart, liver, and intestine were protected from oxidative stress by inhalation of 1–2% H_2 gas (7–11). Interestingly, instead of inhaling H_2 gas, drinking water with dissolved H_2 (H_2-water) protected the brain and kidney from oxidative stress (12–15). These studies strongly suggest the potential of H_2 as an effective therapeutic and preventive antioxidant; however, water dissolves H_2 at 0.8 mmol/l at saturated level. Thus, it has been an open question why consumption of even a small amount of H_2 is effective for various disease models.

Oxidative stress is one of the causes of type 2 diabetes (1–3). To examine whether H_2 has benefits on type 2 diabetes, we used *db/db* mice, in which oxidative stress is accumulated in

the liver and leads to hyperglycemia and hyperlipidemia (23). *Db/db* mice lack a functional leptin receptor, and have been extensively studied as a model for type 2 diabetes (24,25).

In this study, we showed that H_2 can be accumulated in the liver with glycogen after oral administration. Next, chronic consumption of H_2-water reduced oxidative stress in the liver of *db/db* mice, and improved obesity and diabetes. As a mechanistic study, we showed that long-term consumption of H_2-water enhanced the expression of a hepatic hormone, fibroblast growth factor 21 (FGF21), which is a regulator of energy expenditure (26–29). These findings suggest the great potential for hydrogen therapy and prevention of metabolic syndrome.

METHODS AND PROCEDURES

Animals

Male Sprague–Dawley rats of 10 weeks of age and male C57BL/6 mice of 12 weeks of age were purchased from Nippon SLC (Hamamatsu, Shizuoka, Japan). Genetically diabetic male *db/db* mice (BKS.Cg +$Lepr^{db}$/+$Lepr^{db}$/Jcl) and their nondiabetic heterozygous *db*/+ littermates (BKS.Cg m+/+$Lepr^{db}$/Jcl) were purchased at 5 weeks of age from CLEA

[1]Department of Biochemistry and Cell Biology, Institute of Development and Aging Sciences, Graduate School of Medicine, Nippon Medical School, Kawasaki, Kanagawa, Japan; [2]Department of Environmental Gerontology, Tokyo Metropolitan Institute of Gerontology, Itabashi-ku, Tokyo, Japan. Correspondence: Shigeo Ohta (ohta@nms.ac.jp)

Japan, (Tokyo, Japan). Mice were given H$_2$-water from 6 weeks of age. For the diet-induced obesity study, C57BL/6 mice were given a high fat-diet (F2HFD1; Oriental Yeast, Tokyo, Japan) for 1 or 2 weeks. The care and use of laboratory animals were in accordance with the National Institutes of Health guidelines. This study was approved by the Animal Care and Use Committee of Nippon Medical School (Tokyo, Japan).

Hydrogen water

H$_2$-water was prepared as described previously (12). In brief, H$_2$ was dissolved in water under high pressure (0.4 MPa) to a supersaturated level and the saturated H$_2$-water was stored under atmospheric pressure in an aluminum bag with no dead volume. Saturated H$_2$-water was used as 100% H$_2$-water. H$_2$-water degassed by gentle stirring was used as control water. Saturated H$_2$-water was diluted with ninefold control water and used as 10% saturated H$_2$-water. Mice were given water freely using closed glass vessels equipped with an outlet line containing two ball bearings, which kept the water from being degassed. The vessel was freshly refilled with H$_2$-water at 2:00 PM every day.

Diet restriction

Diabetic mice were subjected to controlled dietary restriction, such that the daily diet consumption was equivalent to 80% or 50% of that of *ad libitum* diet consumption. Control groups were permitted free access to food and water throughout the experiment. In the diet-restricted group, mice were permitted *ad libitum* water, but food intake was restricted.

Measurement of H$_2$ concentration

H$_2$ concentration in rat liver tissue was measured using a needle-type hydrogen electrode (Unisense, Aarhus, Denmark). Rat received H$_2$-water orally by stomach gavage at 15 ml/kg. Throughout the experiment, the electrode current was measured with a picoammeter (Keithley, Cleveland, Ohio) and H$_2$ concentration was obtained from the calibration curve generated using known levels of H$_2$-saturated saline.

In an *in vitro* experiment, H$_2$ concentration in glycogen, glucose solutions, or drinking water in the glass vessel was measured using a needle-type hydrogen electrode as described above.

Sample collection and biochemical analysis

Mice were killed under anesthesia, blood was collected from the heart, and liver tissues were excised and frozen with liquid nitrogen or fixed with 4% paraformaldehyde for further analysis. The antioxidation effect of H$_2$ was determined by measuring lipid peroxides in the liver, using a malondialdehyde assay kit (Northwest Life Science Specialties, Vancouver, WA) and the level of lipid peroxides was expressed as nmol malondialdehyde (MDA)/mg protein. Plasma concentrations of total ketone bodies, triglyceride, and total cholesterol were determined with commercially available kits (Wako Pure Chemical Industries, Osaka, Japan). Plasma low-density lipoprotein-cholesterol and high-density lipoprotein-cholesterol were measured using kits (Sekisui Medical, Tokyo, Japan). Plasma glucose and nonesterified fatty acids were determined with kits available from Shino-Test (Tokyo, Japan) and Eiken Chemical (Tokyo, Japan), respectively. Plasma insulin was measured using an insulin ELISA kit (Morinaga Institute of Biological Science, Kanagawa, Japan).

Oil Red O staining

Mouse livers were fixed in 4% paraformaldehyde in phosphate-buffered saline, embedded, and cryosectioned 10 mm thick. The sections were rinsed with 60% isopropanol, stained with 0.25% Oil Red O solution, rinsed with 60% isopropanol, and mounted in aqueous mountant. The area of stained lipid (%) was calculated using the Image J program (ver 1.41; National Institutes of Health, Bethesda, MD) from four sections for each mouse.

Body fat composition analysis

For computed tomography analysis of body fat composition, mice were anesthetized with halothane in a mixture of nitrous oxide and oxygen (70%:30%, vol/vol) and then scanned using a LaTheta LCT-100,

experimental animal computed tomography system (Aloka, Tokyo, Japan). Contiguous 1-mm slice images were used for quantitative assessment using LaTheta software (ver 1.00). Visceral fat, subcutaneous fat, and muscle were distinguished and evaluated quantitatively.

RNA isolation and reverse transcriptase-PCR

Total RNA was isolated from the liver tissue using an RNeasy Mini kit (QIAGEN, Valencia, CA). Complementary DNA generated by SuperScript II Reverse Transcriptase (Invitrogen, Carlsbad, CA) was analyzed by quantitative PCR using Thermal Cycler Dice Real Time System TP800 (TAKARA BIO, Shiga, Japan). All samples were normalized to glyceraldehyde 3-phosphate dehydrogenase expression. Primer and probe sequences for each PCR are shown in Table 1.

Behavioral analysis

Movement activities were recorded in *db/+* and *db/db* mice automatically using a laboratory animal monitoring system (ACTIMO-100; Shinfactory, Fukuoka, Japan). Mice were housed individually and temperature was maintained at 22 °C. Food and water with or without hydrogen were available *ad libitum*. Mice were acclimatized to the chambers for 24 h before beginning recordings and then monitored for 48 h. Movement activity was measured as ambulatory counts from a record of consecutive adjacent infrared beam breaks. Cumulative ambulatory counts on the x- and y-axes were recorded every 10 min.

Indirect calorimetric analyses

Metabolic rate was measured by indirect calorimetric analysis in *db/+* and *db/db* mice using an open-circuit calorimeter (Oxymax; Columbus Instruments, Columbus, OH). Mice were housed individually in a chamber (20 × 10 × 12.7 cm) and temperature was maintained at 22 °C, with air flow of 0.5 l/min. Food and water with or without H$_2$ were available *ad libitum*. Mice were acclimatized to the chambers for 48 h before beginning recordings and then monitored for 48 h. VO_2 and VCO_2 were measured every 10 min using an electrochemical O$_2$ analyzer and a CO$_2$ sensor (Oxymax), and the respiratory exchange ratio was calculated as VCO_2/VO_2 (volume of CO$_2$ produced per volume of O$_2$ consumed (ml/kg/h)).

Statistical analysis

We performed statistical analysis using StatView software (SAS Institute) by applying an unpaired two-tailed Student's *t*-test and ANOVA followed by Fisher's exact test, as described previously (7). Differences were considered statistically significant at $P < 0.05$.

Table 1 Primers and probes for reverse transcriptase-PCR

Gene		Sequence
FGF21	F primer	5'-CCGCAGTCAGAAAGTCTCCT-3'
	R primer	5'-TCTGAAGCTGCAGGCCTCA-3'
	Probe	5'-AGCTCTCTATGGATCGCCTCACTTTGATCC-3'
PEPCK	F primer	5'-TGCTGCAGAACACAAGGGC-3'
	R primer	5'-TTTGCCGAAGTTGTAGCCG-3'
	Probe	5'-TCATCATGCACGACCCCTTTGCC-3'
G6PC	F primer	5'-CGCCATGCAAAGGACTAGGA-3'
	R primer	5'-AGGGCCGATGTCAACACCT-3'
	Probe	5'-TAAAGCCTCTGAAACCCATTGTGAGGCC-3'
GAPDH	F primer	5'-CATCACTGCCACCCAGAAGA-3'
	R primer	5'-ATGTTCTGGGCAGCC-3'
	Probe	5'-TGGATGGCCCCTCTGGAAAGCTG-3'

FGF21, fibroblast growth factor 21; GAPDH, glyceraldehyde 3-phosphate dehydrogenase; G6PC, glucose-6-phosphatase, catalytic subunit; PEPCK, phosphoenolpyruvate carboxykinase.

RESULTS

Molecular hydrogen is accumulated
in the liver with glycogen

We monitored the dynamic movement of H_2 in the liver after oral administration of H_2-water. Rat received H_2-water orally by stomach gavage, and levels of H_2 in the liver were monitored by directly inserting a needle-type hydrogen sensor into the liver for an hour (**Figure 1a**). The H_2 concentration profile gave a peak 5 min after administration of H_2-water in both a fed and fasted liver; however, a great difference was found between the fed and fasted liver; the maximum H_2 level in the fed liver was twofold that of the fasted liver. Moreover, the fed liver maintained a considerable H_2 level for an hour, while that in the fasted liver returned to the basal level after 25 min.

Since a fed liver is rich in glycogen, we speculated that higher polymers of carbohydrates including glycogen have the capacity to maintain H_2. To verify this speculation, we examined saturated solubilities of H_2 in glycogen and glucose solutions by a hydrogen sensor. H_2 was dissolved in a glycogen or glucose solution by bubbling H_2 gas up to a saturated level (**Figure 1b**). Compared to the glucose solution and water, the glycogen solution dissolved a significantly higher amount of
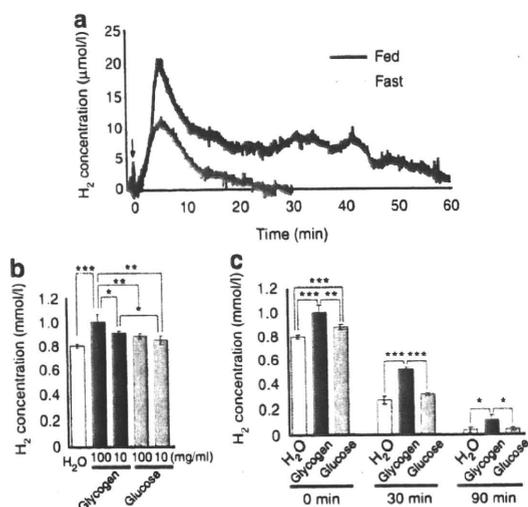
H_2. The hydrogen sensor was not influenced by glycogen and glucose (data not shown). In addition, H_2 was maintained for a longer time in saturated glycogen solution than in saturated glucose solution or water in a plastic tube with the lid off under atmospheric pressure (**Figure 1c**). The half-life was 19.1 ± 2.3, 30.9 ± 3.0, and 20.3 ± 0.4 min (mean $\pm$ s.d., $n = 3$) in water, $100\,mg/ml$ glycogen and glucose solutions, respectively. The half-life of dissolving H_2 in the glycogen solution was prolonged 1.6-fold. Thus, it is concluded that H_2 can be accumulated and reserved in the liver with glycogen, suggesting that expenditure of glycogen should accompany the release of H_2.

Consuming hydrogen water reduces oxidative
stress in the liver and improves fatty liver

Since obesity is a proinflammatory disease, consumption of H_2-water may suppress obesity by acting as an anti-inflammatory. To examine the antioxidation effect of H_2 on the liver, we used obesity and type 2 diabetes model mice *db/db* lacking functional leptin receptors, because oxidative stress is accumulated in the liver. *Db/db* mice and their lean littermates drank H_2-water *ad libitum* for 3 months. H_2-water was exchanged for fresh saturated or 10% saturated water at $1400\,h$ every day. The concentration of dissolved H_2 was measured as described in Methods and Procedures (**Figure 2a**). Since *db/db* mice drank much more water than wild-type mice, H_2 was degassed much faster into the air phase in the vessel used for *db/db* mice; however, a considerable amount of H_2 was maintained by this method.

The effect of H_2 on oxidative stress in the liver was examined as judged by the level of malondialdehyde (MDA), an oxidative stress marker derived from lipid peroxides. The MDA level in the liver of H_2-administered mice significantly fell to nearly the level in nondiabetes control mice, indicating that consumption of H_2-water *ad libitum* markedly suppressed oxidative stress (**Figure 2b**). A dotted pattern caused by the accumulation of fat disappeared in the liver of *db/db* mice with H_2, compared to control water administered *db/db* mice (**Figure 2c**, insets of upper panels). Oil red O staining indicated that H_2 administration significantly reduced neutral lipid accumulation in the livers of *db/db* mice (**Figure 2b**, lower panels and **Figure 2d**, left graph). Furthermore, even with short-term administration (1–2 weeks), H_2 significantly reduced fat accumulation in the liver of high fat-diet-induced obesity mice using the wild-type (**Figure 2d**, middle and right graph). These data clearly indicate that consumption of H_2 markedly reduces hepatic oxidative stress levels and improves fatty liver in *db/db* as well as diet-induced obesity mice.

Consuming hydrogen water suppressed body-weight
gain and reduced plasma glucose and triglyceride levels

To investigate the effect of H_2 on the obesity of *db/db* mice, body-weight was monitored throughout the experimental period, and body fat mass at 18 weeks old was measured by computerized tomography. Mice were divided randomly into 3 groups. Group I (control) was allowed to freely drink water
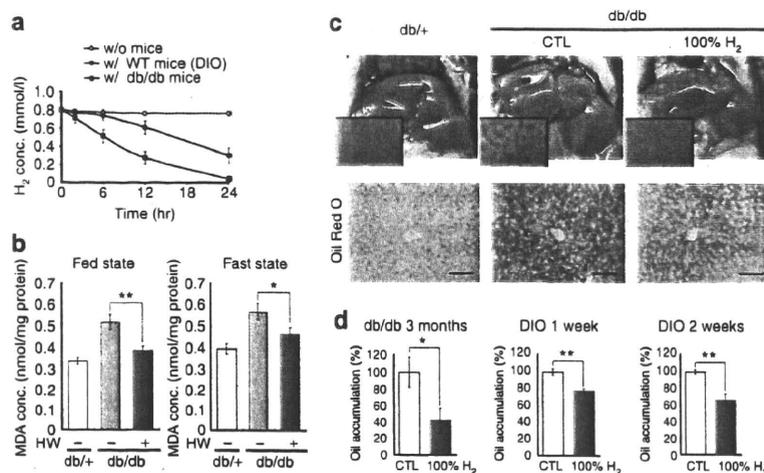

Figure 1 Hydrogen is accumulated and maintained in a fed liver and in glycogen solution *in vitro*. (**a**) The concentration of molecular hydrogen in the liver was monitored using a needle-type hydrogen sensor in fed or overnight-fasted rat liver. Rat received hydrogen water (0.8 mmol/l H_2 in water) orally by stomach gavage at 15 ml/kg. Arrow indicates the time point when rat was administered hydrogen water. (**b**) Saturated concentration of hydrogen in glycogen and glucose solutions, and water. Molecular hydrogen was dissolved in indicated solutions by bubbling H_2 gas to a saturated level. The concentration of hydrogen in solution was measured using a hydrogen sensor. Data are means $\pm$ s.d. ($n = 3$). $^*P < 0.05$; $^{**}P < 0.01$; $^{***}P < 0.001$ compared with 100 or 10 mg/ml glycogen groups. (**c**) Concentration of hydrogen in water, 100 mg/ml glycogen solution and 100 mg/ml glucose solution after bubbling stopped. Hydrogen-saturated solutions were kept in a plastic tube with the lid off at 20 °C for 0, 30, or 90 min under atmospheric pressure. Concentration of hydrogen in solution was measured using a hydrogen sensor. Data are mean $\pm$s.d. ($n = 3$). $^*P < 0.05$, $^{**}P < 0.01$, $^{***}P < 0.001$.

Figure 2 Consuming hydrogen suppresses oxidative stress in the liver and improves fatty liver. (a) Hydrogen concentration in a glass vessel described in Methods and Procedures section was measured without mice (open circle), showing that the equipment retains hydrogen. Profile of the hydrogen concentration in drinking water in a glass vessel given to *db/db* mice (closed square) or wild-type mice used for diet-induced obesity (DIO) (closed circle), indicating that hydrogen gas was released into the air phase by consuming water. Data are the mean ± s.d. ($n = 3$). (b) Malondialdehyde concentration in a fed or overnight-fasted liver was measured. The *db/+* and *db/db* mice were given water with or without hydrogen for 3 months. Data are mean ± s.e.m. ($n = 10$ for each *db/+* group and $n = 15$ for each *db/db* group). *$P < 0.05$, **$P < 0.01$. (c) The appearance and representative oil red O staining of the liver of *db/+* and *db/db* mice given water with and without hydrogen for 3 months, respectively. Scale bar: 100 μm. (d) Levels of fat accumulation in the liver. The *db/db* mice were given water with or without hydrogen for 3 months (left panel). DIO (high fat-diet induced obesity) mice were given water with or without hydrogen for 1 or 2 weeks (middle or right panel). Oil accumulation in the liver was calculated from oil red O staining using an image analysis program, Image J program. Data are mean ± s.e.m. ($n = 12$ for each *db/db* group and $n = 8$ for each DIO group). *$P < 0.05$, **$P < 0.01$.

without H_2. Group II and Group III were given H_2-water with 0.8 mmol/l (saturated H_2-water; 100%) and 0.08 mmol/l (10% saturated level of H_2), respectively. In the initial phase of the experiment, the weight gains of all group animals were similar, suggesting no toxic effect of H_2-water; however, while the control mice exhibited a progressive weight increase, the mice in both 100% and 10% H_2-administered groups achieved a modest weight increase (Figure 3b). Group II mice (100% H_2) were slimmer and their body-weight was significantly lower than that of Group I mice (control) at 18 weeks of age (Figure 3a,b). The suppression of body-weight gain was observed in mice drinking 10% H_2-water (Group III) (Figure 3b). Body fat was also substantially lower in 100% H_2-consuming mice (Figure 3c,d). Since the consumed amounts and volumes of diet and water did not differ among groups (Figure 3e,f), it is suggested that H_2 consumption stimulates energy metabolism to suppress the gain of fat and body weights.

Next, we performed biochemical examinations of blood. Plasma levels of glucose and insulin were significantly reduced in the 100% H_2-administered group and triglycerides were significantly lowered in both 100% and 10% H_2-administered groups (Figure 4a–c). Plasma total ketone bodies tended to increase in the 100% H_2-administered group (Figure 4d), while no change in plasma levels of free fatty acid, high-density lipoprotein-cholesterol, low-density lipoprotein-cholesterol-cholesterol, total cholesterol, and adiponectin was found (Figure 4e–i). These data demonstrate that the consumption of H_2 markedly improves obesity, hyperglycemia, and the plasma triglycerides of diabetic *db/db* mice.

Consuming hydrogen water shows a similar effect to diet restriction

Since *db/db* mice cannot regulate their appetite to eat excess diet by a deficient leptin receptor gene, diet restriction should be effective to improve obesity and diabetes (30). When *db/db* mice were subjected to controlled dietary restriction, the levels of plasma glucose, insulin, and triglycerides significantly fell (Figure 5a–c). When comparing the effects by drinking H_2-water and dietary restriction, the plasma glucose level of mice given 80% of *ad libitum* diet consumption was the same as that of H_2-administered mice (Figure 5a). Furthermore, an additive effect was observed when mice were given both H_2-water and a restricted diet (Figure 5a). A similar additive effect was seen in plasma triglyceride levels (Figure 5c). In particular, when both H_2-water and 80% diet restriction were given to *db/db* mice, the plasma triglyceride reached the level of control *db/+* mice (Figure 5c).

Consuming hydrogen water increases hepatic mRNA level of FGF21

The liver plays an essential role in controlling blood glucose levels by modulating glucose catabolism and gluconeogenesis. To understand the mechanism of how H_2 regulates glucose and triglycerides, *db/db* mice given H_2-water for 3 months were subjected to expression analyses of genes related with the regulation of gluconeogenesis. Phosphoenolpyruvate carboxykinase catalyzes the initial step of gluconeogenesis, and glucose-6-phosphatase catalyzes the last committed step of this process (31). Data from real-time PCR revealed that H_2 administration had no influence on hepatic mRNA levels of
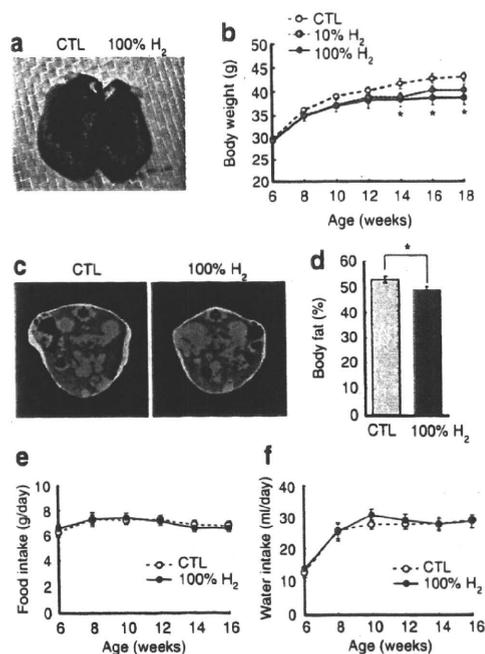
Figure 3 Consuming molecular hydrogen suppresses obesity. (**a**) The appearance of *db/db* mice given water with or without hydrogen for 3 months. Each average mouse was photographed. (**b**) Body weights of *db/db* mice given water with 100% (0.8 mmol/l) or 10% (0.08 mmol/l) hydrogen were examined every 2 weeks. Control mice (CTL) received water without hydrogen. $*P < 0.05$; 100% H_2 vs. control group ($n = 9$ for H_2 and $n = 6$ for control group). (**c**) Representative CT images of abdominal part of average *db/db* mice drinking water with or without hydrogen for 3 months. Blue, green, and red represent visceral fat, subcutaneous fat, and muscle, respectively. (**d**) Total body fat composition of *db/db* mice calculated by the integration of fat area in each section from CT scan images. Data are mean ± s.e.m. ($n = 15$). $*P < 0.05$. (**e**) Food and (**f**) water intake of *db/db* mice was measured every 2 weeks throughout the experiment.
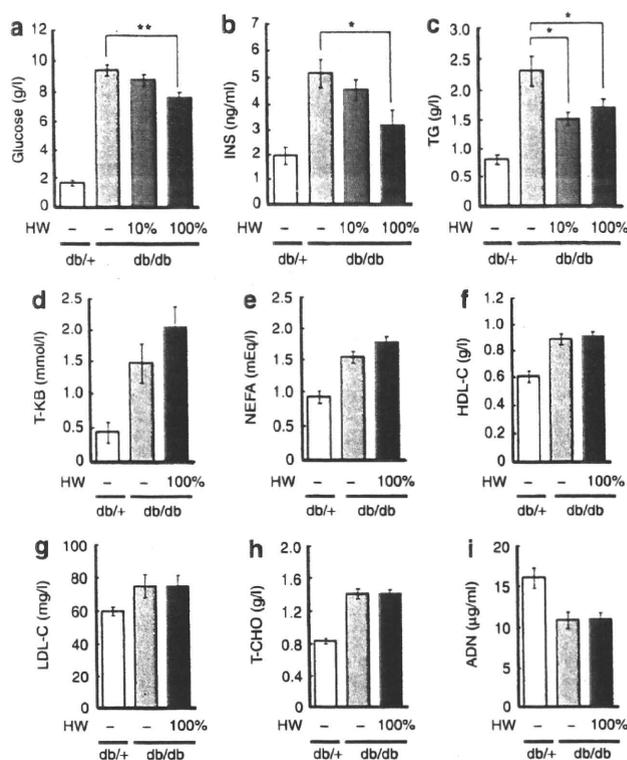

Figure 4 Consuming molecular hydrogen suppresses hyperglycemia, hyperinsulinemia, and plasma triglyceride level. *Db/db* mice were given water with 100% (0.8 mmol/l) or 10% (0.08 mmol/l) hydrogen for 3 months. *Db/+* and *db/db* mice were given water without hydrogen (HW) for the same period as controls. Biochemical analyses were performed to obtain plasma parameters of *db/+* and *db/db* mice. (**a**) Plasma concentration of glucose, (**b**) insulin, (**c**) triglyceride (TG), (**d**) total ketone bodies (T-KB), (**e**) free fatty acids (NEFA), (**f**) high-density lipoprotein-cholesterol (HDL-C), (**g**) low-density lipoprotein-cholesterol-cholesterol (LDL-C), (**h**) total cholesterol (T-CHO), and (**I**) adiponectin (ADN) are shown as mean ± s.e.m. ($n = 15$). $*P < 0.05$, $**P < 0.01$.

phosphoenolpyruvate carboxykinase and glucose-6-phosphatase, catalytic subunit (G6PC) (Figure 6c,d).

Since FGF21, an atypical member of the fibroblast growth factor family, contributes to energy metabolism, we focused on the gene expression of FGF21 after integrated study of the gene expression. H_2 administration induced hepatic mRNA levels of FGF21, regardless of a fed or fasted liver (Figure 6a,b). These results indicate that, at least in part, the induction of hepatic FGF21 contributes to the lowering effect on plasma glucose and triglyceride levels.

Drinking hydrogen water stimulates energy metabolism

To verify whether drinking H_2-water stimulates energy metabolism, we examined oxygen (O_2) consumption and carbon dioxide (CO_2) production. First, we compared physical ability by detecting the movement of mice with infrared beams. Although *db/db* mice was apparently less active in light and dark than control *db/+* mice, no difference was found between *db/db* mice with and without H_2-water (Figure 7a,b).

Db/db mice with or without H_2-water consumed less O_2 and produced less CO_2 than *db/+* control mice (Figure 7c–f).

Moreover, it is significant that H_2-drinking *db/db* mice consumed more O_2, 10%, and produced more CO_2, 10%, than *db/db* mice without H_2-water during both night and day (Figure 7c–f). Since respiratory exchange rates (VCO_2/VO_2) did not differ between *db/db* mice with and without H_2-water, the carbon source for energy production was not changed to stimulate energy metabolism (Figure 7g,h).

Thus, drinking H_2-water suppresses the gain of fat and body weights and improves metabolic parameters by stimulating energy metabolism.

DISCUSSION

In this study, we show a novel benefit of H_2, it may be useful on therapy for and prevention of obesity and diabetes. So far, many reports have confirmed that consumption of H_2 reduces oxidative stress in various disease models and clinical tests (7,8,10–16,19). Clinical tests revealed that drinking H_2-water reduced oxidative stress makers in patients with type 2 diabetes (19) or subjects with potential metabolic syndrome (20), and influenced glucose (19) and cholesterol metabolism (20).
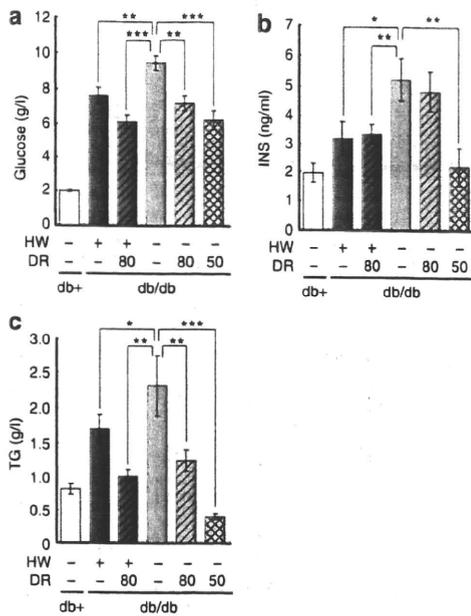
Figure 5 The effect of hydrogen is similar to that of dietary restriction. *Db/db* mice were given water with or without hydrogen (HW) and subjected to dietary restriction (DR). Control groups were permitted free access to food and water throughout the experiment. In diet-restricted groups, mice were permitted *ad libitum* water, but food intake was restricted to 80% or 50% of that of *ad libitum* diet consumption. Plasma concentrations of (a) glucose, (b) insulin (INS), and (c) triglyceride (TG) were measured after 3-month treatment. Data are mean ± s.e.m. *P < 0.05; **P < 0.01; ***P < 0.001; compared with HW (–)/DR (–) group (n = 8–15).

Figure 6 Chronic effects of hydrogen on fibroblast growth factor 21 (FGF21) gene expression in the liver. *Db/+* and *db/db* mice were given water with or without hydrogen for 3 months. (a) The gene expression of FGF21 with fed liver, (b) FGF21 with fast liver, (c) Phosphoenolpyruvate carboxykinase (PEPCK), and (d) glucose-6-phosphatase, catalytic subunit (G6PC) were measured. Data are mean ± s.e.m. *P < 0.05; control vs. hydrogen water in *db/db* mice (n = 15).
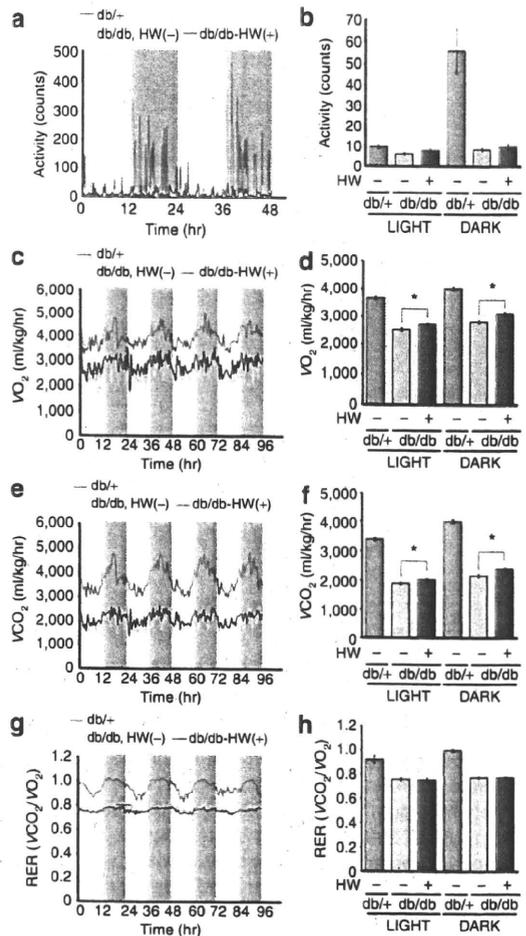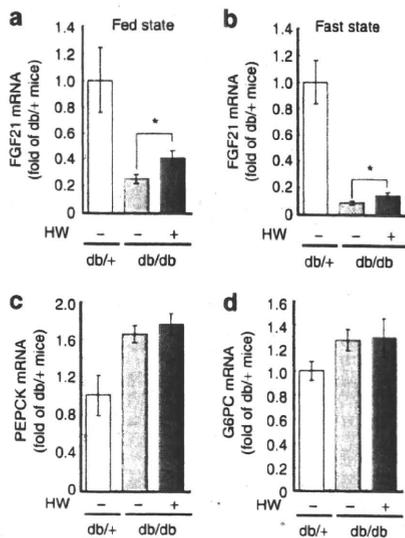

Figure 7 Molecular hydrogen increases oxygen consumption and carbon dioxide production without influencing movement activities. (a and b) movement activity, (c and d) oxygen consumption, (e and f) carbon dioxide production, and (g and h) RER (respiratory exchanging rate) in *db/+* and *db/db* mice given water with or without 100% (0.8 mmol/l) hydrogen for 3 months. (a, c, e, and g) Representative profiles for each parameter. Gray area represent dark phase. (b, d, f, and h) Data are the mean ± s.e.m. (n = 9 and n = 6, for *db/db* and for *db/+* groups, respectively). *P < 0.05.

The mitochondria are a major source of reactive oxygen species during energy production metabolism and H_2 directly protects mitochondria that are exposed to reactive oxygen species (7). Thus, it may be reasonable that mitochondrial energy metabolism, especially fatty acid metabolism, functions against oxidative stress to efficiently expend glucose and fatty acid.

Initially, H_2 was dissolved in culture media and shown to protect cells and organelles by directly reacting highly active reactive oxygen species (7). Next, the brain, heart, liver, and intestine were protected from oxidative stress by inhalation of H_2 gas (7–11). Interestingly, instead of inhaling H_2 gas, H_2-water was effective in protecting the brain and kidney from oxidative stress (12–15) and decreased oxidative stress markers of patients with diabetes and potential metabolic syndrome (19,20). Drinking H_2-water is the most convenient method to

consume H_2; however, when H_2 is consumed from H_2-water, a very limited amount of H_2 can be consumed, because H_2 is dissolved in water at a saturated level of only 0.8 mmol/l under atmospheric pressure. After H_2-water is consumed, most H_2 in blood becomes undetectable within 30 min (14), probably *via* expiration from the lungs; thus, it has been an open question why H_2-water is effective despite its small amount and short exposure. In this study, it was found that H_2 can be accumulated and reserved in the liver with glycogen, which at least partly explains this question.

Moreover, it has been reported that H_2 acts as an anti-inflammatory and antiallergic regulator by inducing inflammatory cytokines, such as tumor necrosis factor-α, interleukin-6 and some phosphorylating signal factors (9,10,14,32). On the other hand, the concept that obesity is a proinflammatory disease has been accepted (33); thus, consumption of H_2-water may suppress obesity by acting as an anti-inflammatory.

Alternatively, we found that consumption of H_2-water enhanced the expression of FGF21. Since it has not been shown that H_2 directly regulates transcription, H_2 is indirectly involved in FGF21 expression. Since FGF21 is a metabolic hormone that improves insulin sensitivity and glucose clearance, reduces plasma triglyceride concentrations and suppresses weight gain when fed a high-fat diet (26–29), all the findings shown in this study were elucidated by the enhanced expression of FGF21.

Indeed, we revealed that drinking H_2-water stimulates energy metabolism as measured by O_2 consumption and CO_2 production. The enhancement of energy metabolism may fully elucidate why consumption of H_2-water suppresses the gain of fat and body weights and improves metabolic parameters; however, it remains unknown whether the induction of FGF21 fully elucidates the enhancement of energy metabolism. Moreover, the relationships among the reduction of oxidative stress, induction of FGF21 expression and stimulation of energy metabolism are still unclear. It should be analyzed whether these relationships are direct or indirect. It might be valuable to examine the relationship of obesity with oxidative stress. Although the primary target of H_2 essentially remains unknown, these findings provide a clue to understand the mechanism of chronic treatment with H_2-water.

Finally, we would like to emphasize that the novel benefit of H_2 in therapeutic and preventive applications for metabolic syndrome could be achieved by the most convenient way, H_2-water.

DISCLOSURE
The authors declared no conflict of interest.

REFERENCES
1. Pérez-Matute P, Zulet MA, Martínez JA. Reactive species and diabetes: counteracting oxidative stress to improve health. *Curr Opin Pharmacol* 2009;9:771–779.
2. Roberts CK, Sindhu KK. Oxidative stress and metabolic syndrome. *Life Sci* 2009;84:705–712.
3. Reddy VP, Zhu X, Perry G, Smith MA. Oxidative stress in diabetes and Alzheimer's disease. *J Alzheimers Dis* 2009;16:763–774.
4. Fearon IM, Faux SP. Oxidative stress and cardiovascular disease: novel tools give (free) radical insight. *J Mol Cell Cardiol* 2009;47:372–381.
5. Tsang AH, Chung KK. Oxidative and nitrosative stress in Parkinson's disease. *Biochim Biophys Acta* 2009;1792:643–650.
6. Henchcliffe C, Beal MF. Mitochondrial biology and oxidative stress in Parkinson disease pathogenesis. *Nat Clin Pract Neurol* 2008;4:600–609.
7. Ohsawa I, Ishikawa M, Takahashi K et al. Hydrogen acts as a therapeutic antioxidant by selectively reducing cytotoxic oxygen radicals. *Nat Med* 2007;13:688–694.
8. Fukuda K, Asoh S, Ishikawa M et al. Inhalation of hydrogen gas suppresses hepatic injury caused by ischemia/reperfusion through reducing oxidative stress. *Biochem Biophys Res Commun* 2007;361:670–674.
9. Nakao A, Kaczorowski DJ, Wang Y et al. Amelioration of rat cardiac cold ischemia/reperfusion injury with inhaled hydrogen or carbon monoxide, or both. *J Heart Lung Transplant* 2010;29:544–553.
10. Buchholz BM, Kaczorowski DJ, Sugimoto R et al. Hydrogen inhalation ameliorates oxidative stress in transplantation induced intestinal graft injury. *Am J Transplant* 2008;8:2015–2024.
11. Hayashida K, Sano M, Ohsawa I et al. Inhalation of hydrogen gas reduces infarct size in the rat model of myocardial ischemia-reperfusion injury. *Biochem Biophys Res Commun* 2008;373:30–35.
12. Nagata K, Nakashima-Kamimura N, Mikami T, Ohsawa I, Ohta S. Consumption of molecular hydrogen prevents the stress-induced impairments in hippocampus-dependent learning tasks during chronic physical restraint in mice. *Neuropsychopharmacology* 2009;34:501–508.
13. Nakashima-Kamimura N, Mori T, Ohsawa I, Asoh S, Ohta S. Molecular hydrogen alleviates nephrotoxicity induced by an anti-cancer drug cisplatin without compromising anti-tumor activity in mice. *Cancer Chemother Pharmacol* 2009;64:753–761.
14. Cardinal JS, Zhan J, Wang Y et al. Oral hydrogen water prevents chronic allograft nephropathy in rats. *Kidney Int* 2010;77:101–109.
15. Fujita K, Seike T, Yutsudo N et al. Hydrogen in drinking water reduces dopaminergic neuronal loss in the 1-methyl-4-phenyl-1,2,3,6-tetrahydropyridine mouse model of Parkinson's disease. *PLoS ONE* 2009;4:e7247.
16. Fu Y, Ito M, Fujita Y et al. Molecular hydrogen is protective against 6-hydroxydopamine-induced nigrostriatal degeneration in a rat model of Parkinson's disease. *Neurosci Lett* 2009;453:81–85.
17. Ohsawa I, Nishimaki K, Yamagata K, Ishikawa M, Ohta S. Consumption of hydrogen water prevents atherosclerosis in apolipoprotein E knockout mice. *Biochem Biophys Res Commun* 2008;377:1195–1198.
18. Oharazawa H, Igarashi T, Yokota T et al. Protection of the retina by rapid diffusion of hydrogen: administration of hydrogen-loaded eye drops in retinal ischemia-reperfusion injury. *Invest Ophthalmol Vis Sci* 2010;51:487–492.
19. Kajiyama S, Hasegawa G, Asano M et al. Supplementation of hydrogen-rich water improves lipid and glucose metabolism in patients with type 2 diabetes or impaired glucose tolerance. *Nutr Res* 2008;28:137–143.
20. Nakao A, Toyoda Y, Sharma P, Evans M, Guthrie N. Effectiveness of hydrogen rich water on antioxidant status of subjects with potential metabolic syndrome-an open label pilot study. *J Clin Biochem Nutr* 2010;46:140–149.
21. Nakayama M, Kabayama S, Nakano H et al. Biological effects of electrolyzed water in hemodialysis. *Nephron Clin Pract* 2009;112:c9–15.
22. Suzuki Y, Sano M, Hayashida K et al. Are the effects of α-glucosidase inhibitors on cardiovascular events related to elevated levels of hydrogen gas in the gastrointestinal tract? *FEBS Lett* 2009;583:2157–2159.
23. Kumashiro N, Tamura Y, Uchida T et al. Impact of oxidative stress and peroxisome proliferator-activated receptor γ coactivator-1α in hepatic insulin resistance. *Diabetes* 2008;57:2083–2091.
24. Coleman DL. Obese and diabetes: two mutant genes causing diabetes-obesity syndromes in mice. *Diabetologia* 1978;14:141–148.
25. Leibel RL, Chung WK, Chua SC Jr. The molecular genetics of rodent single gene obesities. *J Biol Chem* 1997;272:31937–31940.

26. Reitman ML. FGF21: a missing link in the biology of fasting. *Cell Metab* 2007;5:405–407.

27. Kharitonenkov A, Shiyanova TL, Koester A *et al*. FGF-21 as a novel metabolic regulator. *J Clin Invest* 2005;115:1627–1635.

28. Kharitonenkov A, Wroblewski VJ, Koester A *et al*. The metabolic state of diabetic monkeys is regulated by fibroblast growth factor-21. *Endocrinology* 2007;148:774–781.

29. Kharitonenkov A, Shanafelt AB. FGF21: a novel prospect for the treatment of metabolic diseases. *Curr Opin Investig Drugs* 2009;10: 359–364.

30. Lee SM, Bressler R. Prevention of diabetic nephropathy by diet control in the db/db mouse. *Diabetes* 1981;30:106–111.

31. Ruderman NB. Muscle amino acid metabolism and gluconeogenesis. *Annu Rev Med* 1975;26:245–258.

32. Itoh T, Fujita Y, Ito M *et al*. Molecular hydrogen suppresses FcepsilonRI-mediated signal transduction and prevents degranulation of mast cells. *Biochem Biophys Res Commun* 2009;389:651–656.

33. Aggarwal BB. Targeting inflammation-induced obesity and metabolic diseases by curcumin and other nutraceuticals. *Annu Rev Nutr* 2010;30:173–199.